UC Santa Barbara
UC Santa Barbara Previously Published Works

Title

Synthesis and biological characterization of a promising F-18 PET tracer for vesicular acetylcholine transporter

Permalink

https://escholarship.org/uc/item/0gc0m2w2

Journal

Bioorganic & Medicinal Chemistry, 23(15)

ISSN

0968-0896

Authors

Tu, Zhude
Zhang, Xiang
Jin, Hongjun
et al.

Publication Date

2015-08-01

DOI

10.1016/j.bmc.2015.05.058

Peer reviewed

Synthesis and Biological Characterization of a Promising F-18 PET Tracer for Vesicular Acetylcholine Transporter

Zhude Tu[a,*], **Xiang Zhang**[a], **Hongjun Jin**[a], **Xuyi Yue**[a], **Prashanth K. Padakanti**[a], **Lihai Yu**[a], **Hui Liu**[a], **Hubert P. Flores**[b], **Kota Kaneshige**[c], **Stanley M. Parsons**[c], and **Joel S. Perlmutter**[a,b]

[a]Department of Radiology, Washington University School of Medicine, 510 South Kingshighway Blvd., St. Louis, MO 63110, USA

[b]Department of Neurology, Washington University School of Medicine, 510 South Kingshighway Blvd., St. Louis, MO 63110, USA

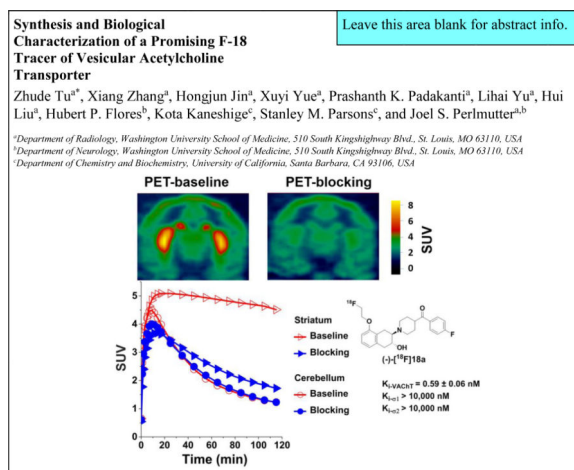[c]Department of Chemistry and Biochemistry, University of California, Santa Barbara, CA 93106, USA

Abstract

Nine fluorine-containing vesicular acetylcholine transporter (VAChT) inhibitors were synthesized and screened as potential PET tracers for imaging the VAChT. Compound **18a** was one of the most promising carbonyl-containing benzovesamicol analogues; the minus enantiomer, (-)-**18a** displayed high potency (VAChT $K_i = 0.59 \pm 0.06$ nM) and high selectivity for VAChT versus receptors (> 10,000-fold). The radiosynthesis of (-)-[^{18}F]**18a** was accomplished by a two-step procedure with 30 – 40% radiochemical yield. Preliminary biodistribution studies of (-)-[^{18}F]**18a** in adult male Sprague–Dawley rats at 5, 30, 60 and 120 min post-injection (p.i.) were promising. The total brain uptake of (-)-[^{18}F]**18a** was 0.684 ID%/g at 5 min p.i. and by 120 min p.i. slowly washed out to 0.409 %ID/g.; evaluation of regional brain uptake showed stable levels of ~0.800 %ID/g from 5 to 120 min p.i in the VAChT-enriched striatal tissue of rats, indicating the tracer had crossed the blood brain barrier and was retained in the striatum. Subsequent microPET brain imaging studies of (-)-[^{18}F]**18a** in nonhuman primates (NHPs) showed high striatal accumulation in the NHP brain; the standardized uptake value (SUV) for striatum reached a maximum value of 5.1 at 15 min p.i. The time-activity curve for the target striatal region displayed a slow and gradual decreasing trend 15 min after injection, while clearance of the radioactivity from the cerebellar reference region was much more rapid. Pretreatment of NHPs with 0.25 mg/kg of the VAChT inhibitor (-)-vesamicol resulted in a ~90% decrease of striatal uptake compared to baseline studies. HPLC metabolite analysis of NHP plasma revealed that (-)-[^{18}F]**18a** had a good *in vivo* stability. Together, these preliminary results suggest (-)-[^{18}F]**18a** is a promising PET tracer candidate for imaging VAChT in the brain of living subjects.

---

*Corresponding author. Tel.: +1-314-362-8487; fax: +1-314-362-8555. tuz@mir.wustl.edu (Z. Tu).

Graphical Abstract

Synthesis and Biological Characterization of a Promising F-18 Tracer of Vesicular Acetylcholine Transporter

Leave this area blank for abstract info.

Zhude Tu[a*], Xiang Zhang[a], Hongjun Jin[a], Xuyi Yue[a], Prashanth K. Padakanti[a], Lihai Yu[a], Hui Liu[a], Hubert P. Flores[b], Kota Kaneshige[c], Stanley M. Parsons[c], and Joel S. Perlmutter[a,b]

[a]Department of Radiology, Washington University School of Medicine, 510 South Kingshighway Blvd., St. Louis, MO 63110, USA
[b]Department of Neurology, Washington University School of Medicine, 510 South Kingshighway Blvd., St. Louis, MO 63110, USA
[c]Department of Chemistry and Biochemistry, University of California, Santa Barbara, CA 93106, USA

Keywords

VAChT; PET tracer; Vesamicol; F-18; Striatum

1. Introduction

The loss or decline in memory and other cognitive abilities is a clinical syndrome characteristic of dementia which is common seen in Alzheimer disease (AD), Parkinson Disease (PD), and other neurodegenerative diseases.[1-6] The severity of dementia is linked to loss of cholinergic neurons and synapses in the central nervous system (CNS). Identifying a reliable biomarker that is able to assess the loss of the cholinergic neuron is imperative. The vesicular acetylcholine transporter (VAChT) is an important transporter protein in the neuronal cholinergic system and has been accepted as a reliable cholinergic marker for more than 25 years.[7-10] Positron emission tomography (PET) is a non-invasive imaging modality and able to provide functional information for molecular and cellular processes in living subjects. A PET radioligand having high affinity and selectivity for VAChT, and suitable radiopharmaceutical properties would provide a unique tool to measure the loss of cholinergic neurons in the brain of subjects with dementia by assessing changes in VAChT level. The identification of a potent and selective PET ligand with minimal pharmacological effects has posed significant difficulties. Vesamicol (**1**, initially named AH 5183, **Figure 1**) was first reported in 1969 [11, 12] as a potential local anesthetic. Bahr and Parsons reported that L-isomer and D-isomer of vesamicol had a different binding activity in *Torpedo* synaptic vesicles in 1986; vesamicol was later discovered to be a stereoselective inhibitor of VAChT.[13-15] Although tritiated vesamicol has been widely used for *in vitro* studies of cholinergic loss, vesamicol and many analogues have significant binding affinity for receptors that limits their use as VAChT imaging agents because receptors are highly expressed throughout the brain.[16-18] To overcome this challenge, investigators have put tremendous efforts into exploring vesamicol derivatives to improve the imaging of the VAChT binding and to reduce the σ receptor binding affinity. Identification of benzovesamicol (**2**, BVM, **Figure 1**) was a significant achievement, as this structural

modification not only retained the high VAChT affinity, but also offered position(s) on the aromatic ring in the tetralin fragment for introducing substitution group(s).[19-22] Among the benzovesamicol analogues shown in **Figure 1**, 5-(*N*-methyl-amino)benzovesamicol (**3**, MABV) and *N*-ethyl-fluoroacetamidobenzovesamicol (**4**, NEFA) are more potent inhibitors and more selective for VAChT versus σ receptors than vesamicol.[23] Furthermore, the single-photon emission computerized tomography (SPECT) radiotracer (-)-5-[^{123}I]iodo-benzovesamicol ([^{123}I]**5**, [^{123}I]IBVM) was used for mapping cholinergic terminals in the human brain [7-9, 24-27] although quantification of peak uptake in the target regions required at least 6 hr post-injection (p.i.). Although SPECT is a useful tool for studies of ligands with slow kinetic processes,[28] PET offers higher spatial resolution and sensitivity for clinical studies of ligands with more rapid pharmacokinetics. [^{18}F]fluoroethoxy-benzovesamicol ([^{18}F]**6**, [^{18}F]FEOBV) was recently approved for the clinical studies in human subjects as a PET ligand for assessing the VAChT levels in the brain as a biomarker of cholinergic function.[29-32] Although equilibrium kinetics in the brain of both NHP and human subjects show delayed equilibrium of > 360 min p.i.,[32] [^{18}F]FEOBV offers advantages over SPECT ligands for both preclinical and clinical imaging of cholinergic loss. Studies of FEOBV in a rat model of cholinergic dysfunction showed a good correlation between PET measures of [^{18}F]FEOBV uptake and *ex vivo* autoradiography of the same animals post PET; *ex vivo* brain autoradiography measures of [^{18}F]FEOBV binding in human AD cases and age-matched controls also showed differences consistent with cholinergic loss.[33, 34]

We previously reported a new class of VAChT analogues in which a carbonyl group is interposed between the phenyl and piperidine ring of the benzovesamicol structure; several lead candidates displayed high *in vitro* binding affinity and high selectivity for VAChT versus other CNS targets.[35-40] Evaluation of these ^{11}C- and ^{18}F-labeled radiotracers in rodents and microPET imaging studies in NHPs suggested that the radiolabeled version of several ligands (**7-10, Figure 1**) bound *in vivo* to the VAChT enriched striatal regions. [38-41] The half-life of ^{18}F (T$_{1/2}$ = 109.8 min) permits longer scan sessions that generate higher target-to-reference ratios; ^{18}F PET tracers also place fewer time constraints on tracer production. Here we further explore carbonyl-containing benzovesamicol analogues using the following strategies: 1) Incorporating PEGylated groups on the phenyl ring linked to the piperidinyl ring by the carbonyl group (**Figure 1**), which can improve clearance kinetics by decreasing lipophilicity;[42-44] 2) Introducing a fluoroethoxy group on the tetralin moiety to further improve affinity and selectivity for VAChT versus the σ receptors; 3) Incorporating a fluorine atom to provide position(s) for ^{18}F radiolabeling. In this manuscript, we report the synthesis and *in vitro* and *in vivo* biological evaluation of the new fluorinated carbonyl-containing analogues to determine their suitability as ^{18}F labeled ligands for imaging VAChT *in vivo*.

2. Results and Discussion

2.1 Chemistry

The syntheses of the PEGylated compounds **12** – **14** are shown in **Scheme 1**. Intermediate **11** was synthesized as previously reported.[40] Fluoroethoxy-containing **12** was obtained by

O-alkylation of **11** with 2-bromo-1-fluoroethane. PEGylated analogues **13** and **14** were obtained by treating **11** with the corresponding fluorinated PEGylated tosylates. The syntheses of benzovesamicol analogues containing a 5-substituted carbonyl group are shown in **Scheme 2**. The epoxide compound **15** was synthesized as previously described.[36, 38] Commercially available (4-fluorophenyl)(piperidin-4-yl)methanone (**16**) was reacted with **15** to afford the phenol regioisomers **17a** and **17b**. The desired ligands **18a** and **18b** were obtained via *O*-alkylation of **17a** and **17b** respectively with -2-fluoroethyl tosylate.

Since VAChT inhibitors demonstrate stereoselective binding, we initially attempted to resolve the potent racemic compound (±)-**18a** directly using a Chiralcel OD column without success. To overcome this challenge, racemic compound (±)-**18a** was first converted to the acetate ester (±)-**19a**, which was easily resolved on Chiralcel OD column using a mobile phase of 3% 2-propanol in hexanes, as shown in **Scheme 3**. Using a semi-preparative Chiralcel OD column, the minus isomer (-)-**19a** eluted at 25-29 min and the plus isomer (+)-**19a** eluted at 30-38 min. Hydrolysis of the enantiomers (-)-**19a** and (+)-**19a** using saturated sodium carbonate aqueous solution afforded the desired enantiomers (-)-**18a** and (+)-**18a**.

2.2 *In vitro* binding affinity studies

The newly synthesized analogues were screened using our standard *in vitro* binding assays [36, 37, 40, 45] to measure their affinities to VAChT and σ receptors (**Table 1**). [^{3}H]vesamicol was used as the radioligand for the VAChT competitive binding assay; [^{3}H]pentazocine and [^{3}H]ditolylguanidine([^{3}H]DTG) in the presence of 1 μM (+)-pentazocine were used for σ_1 and σ_2 receptor binding assays respectively. PEGylated compounds **12-14** displayed similar binding affinities for VAChT (0.87 to 1.74 nM), while the selectivity for VAChT over both σ_1 and σ_2 receptors was greatly increased by extending the PEG chain: $K_{i\text{-}\sigma1}$ values were 13.23 ± 0.20, 1,580 ± 46, and > 10,000 nM for compounds **12**, **13,** and **14** respectively. In comparison of compounds **17a** to **17b**, and **18a** to **18b**, the hydroxyl or fluoroethoxy substitution on the 8-position resulted in > 10-fold decrease of VAChT affinity with the K_i values of 4.64 ± 0.32, 56.20 ± 4.08 nM for **17a** and **17b**, 1.55 ± 0.18, 92.80 ± 22.20 nM for **18a** and **18b** respectively; the observed stereoselectivity for VAChT is consistent with previous reports.[46, 47] Enantiopure (-)-**18a** was more potent than (+)-**18a** with K_i values of 0.59 ± 0.06, 13.0 ± 2.20 nM for (-)-**18a** and (+)-**18a** respectively. The results of these *in vitro* binding studies suggested that: 1) PEGylation not only reduces the lipophilicity, but also improves selectivity for VAChT versus σ receptors; 2) the 5-substitution of the tetralin moiety provides higher binding affinity for VAChT than the non-substituted compound **10** or the 8-substituted counterpart; the observation that 5-position substituted compounds demonstrated high potency is consistent with literature reports;[46, 47] 3) VAChT binding has stereoselectivity. For racemic compound **18a**, the minus isomer (-)-**18a** is more potent than its plus isomer (+)-**18a**. Enantiopure (-)-**18a** displayed high VAChT binding affinity (0.59 ± 0.06 nM) and high selectivity versus σ receptors (>10,000-fold), and acceptable lipophilicity, with calculated Log*P* value of 3.45. Compound (-)-**18a** was chosen for radiolabeling with ^{18}F and for further evaluation in rodents and nonhuman primates.

2.3 Radiochemistry

The radiosynthesis of (-)-[^{18}F]**18a** was accomplished by a two-step ^{18}F labeling strategy starting with (-)-**17a** as shown in **Scheme 4**. Ethylene ditosylate was first reacted with [^{18}F]KF/Kryptofix 2.2.2 in acetonitrile and then purified on a reversed phase HPLC system to afford [^{18}F]fluoroethyl tosylate ([^{18}F]**20**) with a 60-75% radiochemical yield. Nucleophilic substitution of (-)-**17a** with [^{18}F]**20** in dimethyl sulfoxide (DMSO) followed by HPLC purification afforded (-)-[^{18}F]**18a** in 50-60% radiochemical yield (decay corrected to end of synthesis, n > 20). The radioactive (-)-[^{18}F]**18a** was authenticated by co-injection with the nonradiolabeled standard (-)-**18a** on an analytical HPLC system. The two-step radiosynthesis of (-)-[^{18}F]**18a** took ~ 2.0 hr with overall radiochemical yield of 30 to 40%, specific activity > 74 GBq/μmol (decay corrected to EOS) and radiochemical purity > 98% (n > 20).

2.4 *Ex vivo* autoradiography study in rats

To confirm the target binding selectivity of (-)-[^{18}F]**18a** in the rat brain, *ex vivo* autoradiography was performed. An adult male Sprague-Dawley (SD) rat was euthanized 60 min p.i. The brain was quickly removed and snap-frozen then sectioned at 100 μm and mounted on glass slides. The brain sections were exposed to the film in an imaging cassette for 12 hr; the distribution of radioactivity is shown in **Figure 2** with the outlined regions of interest based on standard anatomical guides.[48] The results show (-)-[^{18}F]**18a** has the highest accumulation in the VAChT enriched striatum, which is consistent with the literature reports.[49] The uptake ratio of radioactivity in striatum versus cerebellum reached 4.19 ± 0.37 at 60 min p.i.

2.5 Biodistribution studies in rats

Biodistribution and regional brain uptake studies of (-)-[^{18}F]**18a** were performed in adult male SD rats at 5, 30, 60, and 120 min p.i.; the results are shown in **Table 2**. The initial uptake (%ID/g) at 5 min p.i. in blood, heart, lung, muscle, fat, pancreas, spleen, kidney, liver, and brain was 0.209, 0.706, 2.255, 0.171, 0.144, 1.202, 1.265, 2.363, 1.065 and 0.684 respectively. The clearance of the radioactivity was rapid from the heart, lung, spleen, kidney, and liver; the uptake (ID%/g) decreased to 0.390, 0.973, 0.685, 0.883, and 0.523, respectively, at 30 min and further decreased at 60 and 120 min p.i. The high initial kidney uptake suggests the radiotracer may be initially excreted through the urinary system. From 5 to 120 min, the bone uptake of the radioactivity remained stable, suggesting that there is no significant metabolic defluorination *in vivo*. For brain regions of interest, the uptake (ID%/g) of the cerebellum, brain stem, cortex, striatum, thalamus, and hippocampus was 0.593, 0.683, 0.777, 0.782, 0.691, and 0.645 respectively at 5 min post injection of (-)-[^{18}F]**18a**; the initial uptake of the striatal region was a little higher than other brain regions but no significant difference was observed, as shown in **Table 2** and **Figure 3**. However, the striatal region retained the highest levels (%ID/g) at 0.886, 0.819, and 0.761 at 30, 60 and 120 min, respectively, in contrast with other brain regions. The uptake ratios for target to non-target brain regions (striatum-to-cerebellum) increased from 1.3-fold at 5 min to 3.0-fold at 30 min and remained steady up to 120 min p.i. as shown in **Figure 3**.

2.6 MicroPET imaging studies in NHPs

Following the promising data from rat *ex vivo* autoradiography and biodistribution studies, microPET imaging of (-)-[^{18}F]**18a** in the brains of male cynomolgus monkeys was used to determine its potential as a PET tracer for imaging the VAChT *in vivo*. As shown in **Figure 4**, the microPET imaging results suggested that (-)-[^{18}F]**18a** was able to enter the NHP brain and had the highest accumulation in the striatal region including both caudate and putamen. This high accumulation of radioactivity in the striatal region further indicates that (-)-[^{18}F]**18a** binds to VAChT *in vivo*. The time-activity curves showed that the radioactivity accumulation in striatum reached maximum with a standardized uptake value (SUV) of 5.1 at 15 min p.i. and decreased slowly over 120 min p.i. Compared with [^{18}F]FEOBV which displayed slow striatal kinetics, (-)-[^{18}F]**18a** demonstrated a much faster equilibrium for striatal binding in NHP. The uptake ratio of the target (striatum) versus non-target (cerebellum) increased gradually and reached ~3.0 at 80 min p.i. To test the specificity of (-)-[^{18}F]**18a** binding to VAChT in the brain, microPET studies were performed in a monkey pretreated with 0.25 mg/kg (-)-vesamicol, a known VAChT inhibitor, 5 min before (-)-[^{18}F]**18a** injection. Striatal uptake in this blocking study was reduced about ~90% compared to the striatal uptake in the baseline condition (**Figure 4**), while the change in the cerebellar region was negligible (**Figure 4**); this further suggested that (-)-[^{18}F]**18a** binds to VAChT specifically in the monkey brain.

2.7 Metabolite studies in NHP plasma

Because the microPET imaging data suggested that (-)-[^{18}F]**18a** was a promising candidate VAChT-specific PET radiotracer, radioactive metabolite analysis was performed in NHP plasma samples post injection of (-)-[^{18}F]**18a**. 70 - 82% of the radioactivity was in the plasma after centrifugation to separate the red blood cells. Following solvent extraction and deproteination, 76 - 87% of the radioactivity in plasma was in the supernatant. The solvent extract was then injected onto HPLC to identify the percentage of radioactive parent compound versus any radiolabeled metabolites. The HPLC metabolite analysis of the plasma samples showed three radioactive peaks: the parent compound (-)-[^{18}F]**18a**, radioactive metabolite 1 and radioactive metabolite 2; the retention times were 9 – 11 min for (-)-[^{18}F]**18a**, 2 – 4 min for the major hydrophilic radioactive metabolite 1 and 6 – 7 min for the radioactive metabolite 2 which represented < 1.5% of the total radioactivity collected from the HPLC and is considered negligible. The percentage of the remaining parent compound (-)-[^{18}F]**18a** was 66, 41, 21, and 16% at 15, 30, 60 and 90 min p.i. respectively. The level of radioactive metabolite 1 was 3.0, 30, 59, 78 and 82% at 5, 15, 30, 60 and 90 min respectively as shown in **Figure 5**. To test if the hydrophilic radioactive metabolite 1 has capability in penetrating the blood brain barrier and thus confound PET measurement, we evaluated the stability of the tracer in rat blood and brain. The radiometabolite analysis of the rat plasma samples revealed that (-)-[^{18}F]**18a** in rat metabolized much faster than in monkeys, indicating the metabolism of (-)-[^{18}F]**18a** has a species difference. This limits the utility of rodent data in predicting the metabolism of (-)-[^{18}F]**18a** in nonhuman primates or human subjects. Future metabolite analysis of the human plasma samples, kinetic modeling of tracer uptake, and clearance in human subjects are necessary to determine if the major radioactive metabolite can enter into the human brain.

3. Experimental

3.1 General

All the solvents and reagents were obtained commercially and used as received, unless otherwise stated. All anhydrous reactions were carried out in oven-dried or flame-dried, and nitrogen purged glassware. Anhydrous tetrahydrofuran was dried over sodium and fresh distilled prior to use. Anhydrous dichloromethane was distilled over calcium hydride prior to use. Reactions were monitored by thin layer chromatography (TLC) using silica gel 60 F_{254} glass plates (EMD Chemicals Inc.). Flash column chromatography was performed over silica gel (32-63 μm), HPLC grade solvents were used for chromatography. ^{1}H NMR were recorded on a Varian Mercury-VX 400 or 300 MHz spectrometer. The chemical shifts are reported as values (ppm) relative to tetramethylsilane (TMS) as an internal reference. The SpectraSystem was used for both analytical and semi-preparative HPLC. A Chiralcel OD normal phase HPLC column was used to resolve enantiomers. The specific optical rotation was determined on an automatic polarimeter (Autopol 111, Rudolph Research, Flanders, NJ). Elemental analyses were determined by Atlantic Microlab, Inc. (Norcross, GA).

[18F]Fluoride was produced from a RDS111 cyclotron (Siemens/CTI Molecular Imaging, Knoxville, TN) by $^{18}O(p, n)^{18}F$ reaction through proton irradiation of enriched ^{18}O water (95%). [18F]Fluoride was firstly passed through an ion-exchange resin and then eluted using 0.02 M potassium carbonate (K_2CO_3) solution.

3.1.1 (4-(2-Fluoroethoxy)phenyl)(1-(3-hydroxy-1,2,3,4-tetrahydronaphthalen-2-yl)piperidin-4-yl)methanone (12)—To a solution of **11** (30 mg, 0.08 mmol) in acetone (10 mL) was added K_2CO_3 (12 mg, 0.08 mmol) and 2-bromo-1-fluoroethane (54 mg, 0.2 mmol). The reaction mixture was refluxed overnight until the reaction was completed as determined by TLC. After the solvent was removed, 20 mL of water was added to the flask, and the mixture was extracted with ethyl acetate (10 mL × 3). The combined organic layers were dried over anhydrous sodium sulfate and concentrated under reduced pressure. The crude product was purified by silica gel column chromatography using ethyl acetate/hexane(1/4, v/v) to give compound **12** (26.1 mg, 77%) as a pale yellow solid. ^{1}HNMR (400 MHz, CDCl$_3$) δ 1.76–1.95 (m, 4 H), 3.88 (dt, J = 2.7, 12.4 Hz, 1 H), 2.75–3.02 (m, 7 H), 3.24-3.35 (m, 2 H), 3.88 (td, J = 5.0, 13.8 Hz, 1 H), 4.05 (t, J = 4.0 Hz, 1 H). 4.33 (t, J = 4.2 Hz, 1 H). 4.71 (t, J = 4.0 Hz, 1 H), 4.87 (t, J = 4.2 Hz, 1 H), 6.99 (d, J = 8.4 Hz, 2 H), 7.09–7.16 (m, 4 H), 7.95 (d, J = 9.0 Hz, 2 H). ^{13}C NMR (75.5 MHz, CD$_3$OD) δ 201.4, 165.9, 162.4, 136.0, 135.0, 131.0, 129.1, 126.2, 116.6, 115.0, 108.6, 82.5 (J = 167.2 Hz), 68.0, 66.3 (d, J = 23.2 Hz), 50.3, 47.0, 43.3, 38.4, 31.2, 29.7, 28.0, 24.3; HRMS (ESI) Calcd for $C_{24}H_{29}FNO_3$ (M+H)$^+$ 398.2131, found: 398.2129. To 26 mg (0.065 mmol) of **12** in a glass vial was added in 2.5 mL of dichloromethane, and 2.94 mg (0.0325 mmol) of oxalic acid in methanol was added. After recrystallization, 31.4 mg of the oxalate salt was obtained, Mp: 196.2 – 197.0 °C.

3.1.2 (4-(2-(2-Fluoroethoxy)ethoxy)phenyl)(1-((2R,3R)-3-hydroxy-1,2,3,4-tetrahydronaphthalen-2-yl)piperidin-4-yl)-methanone (13)—To a solution of **11** (40 mg, 0.11 mmol) in 2.0 mL DMF was added 2-(2-fluoroethoxy)ethyl tosylate (60 mg, 0.22

mmol) and K_2CO_3 (35 mg, 0.25 mmol). The mixture was stirred at room temperature overnight. Ethyl acetate (35 mL) was added into the reaction mixture, and then sequentially washed with saturated $NaHCO_3$ aqueous solution and brine. The combined organic solution was dried over anhydrous sodium sulfate, concentrated under reduced pressure. The crude product was purified on a silica gel column to give compound **13** (38 mg, 78%) as colorless syrup. ^{1}HNMR (400 MHz, CDCl$_3$) δ 7.94 (d, *J*=8.7 Hz, 2H), 7.12 (s br, 4H), 6.98 (d, *J*=8.4 Hz, 2H), 4.70-4.65 (m, 1H), 4.55-4.49 (m, 1H), 4.25-4.20 (m, 2H), 4.00-3.75 (m, 5H), 3.40-3.10 (m, 2H), 3.10-2.70 (m, 7H), 2.5-2.30 (m, 1H), 2.00-1.70 (m, 4H). The oxalate salt was obtained as described above. Mp: 203 – 206 °C. Anal. Calcd of $C_{28}H_{34}FNO_8$: C, 63.27; H, 6.45; N, 2.63. Found: C, 63.29; H, 6.49; N, 2.79. HRMS (ESI) Calcd for $C_{26}H_{33}FNO_4$ (M+H)[+] 442.2394, found: 442.2392.

3.1.3 (4-(2-(2-(2-Fluoroethoxy)ethoxy)ethoxy)phenyl)(1-((2R,-3R)-3-hydroxy-1,2,3,4-tetrahydronaphthalen-2-yl)piperidin-4-yl)methanone (14)—

Following the similar procedure for preparing compound **13**, compound **14** was afforded as colorless oil (41.6 mg, 41%). ^{1}HNMR (400 MHz, CDCl$_3$) δ 7.93 (d, *J*=9.0 Hz, 2H), 7.11 (s br, 4H), 6.97 (d, *J*=9.0 Hz, 2H), 4.70-4.63 (m, 1H), 4.55-4.45 (m, 1H), 4.25-4.18 (m, 3H), 4.00-3.80 (m, 3H), 3.80-3.70 (m, 6H), 3.40-3.20 (m, 2H), 3.10-2.70 (m, 7H), 2.5-2.30 (m, 1H), 2.00-1.70 (m, 4H). The oxalate salt was obtained as described above. Mp: 189.8 – 191.8 °C. Anal. Calcd for $C_{30}H_{38}FNO_9$: C, 62.60; H, 6.65; N, 2.43. Found: C, 62.63; H, 6.62; N, 2.50. HRMS (ESI) Calcd for $C_{26}H_{37}FNO_5$ (M+H)[+] 486.2656, found: 486.2655.

3.1.4 (1-(3,5-Dihydroxy-1,2,3,4-tetrahydronaphthalen-2-yl)-piperidin-4-yl)(4-fluorophenyl)methanone (17a) and (1-(3,8-dihydroxy-1,2,3,4-tetrahydronaphthalen-2-yl)piperidin-4-yl)(4-fluorophenyl)methanone (17b)—

Compound **15** (200 mg, 1.2 mmol), (4-fluorophenyl)(piperidin-4-yl)methanone **16** (585 mg, 2.4 mmol) and triethylamine (1 mL) were mixed in ethanol (5 mL) and heated at 60 °C for 2 d. Ethyl acetate (50 mL) was used to dilute the solution and then washed with brine (2×10 mL). After concentration, the residue was loaded onto silica gel column and eluted using CH_2Cl_2/methanol (20/1, v/v). Compound **17a** was obtained as the first component, a white solid (109 mg, 25%). Mp 229 – 230 °C. ^{1}H NMR (300 MHz, CDCl$_3$) δ 8.00 – 7.94 (m, 2H), 7.15 – 7.11 (m, 2H), 7.02 (t, *J* = 7.8 Hz, 1H), 6.66 (dd, *J* = 25.2 Hz, 7.8 Hz, 2H), 5.01 (br, 1H), 3.92 – 3.83 (m, 1H), 3.32 – 3.23 (m, 2H), 3.07 – 2.97 (m, 2H), 2.89 – 2.77 (m, 4H), 2.64 – 2.45 (m, 2H), 1.97 – 1.89 (m, 3H), 1.88 – 1.76 (m, 1H). ^{13}C NMR (75.5 MHz, CDCl$_3$) δ 201.1, 166.2 (d, *J* = 301.0 Hz), 153.6, 135.8, 130.9, 130.8, 126.9, 121.8, 121.4, 115.8 (d, *J* = 21.7 Hz), 112.1, 66.5, 65.3, 51.9, 43.8, 37.8, 29.5, 29.2, 28.5, 20.0. HRMS (ESI) Calcd for $C_{22}H_{25}FNO_3$ (M+H)[+] 370.1818, found: 370.1817.

Compound **17b** was obtained as the second component, a white solid (120 mg, 27%). Mp 208 – 210 °C. ^{1}H NMR (400 MHz, CDCl$_3$) δ 1.76-1.93 (m, 4H), 2.46-2.64 (m, 2H), 2.76-2.89 (m, 4H), 2.97-3.07 (m, 2H), 3.25-3.32 (m, 2H), 3.88 (s, 1H), 6.61 (d, *J* = 8.4Hz, 2H), 6.72 (d, *J* = 7.5Hz, 1H), 7.15 (t, *J* = 8.1Hz, 2H), 7.98 (t, *J* = 8.4Hz, 2H). ^{13}C NMR (75.5 MHz, CD_3SOCD_3) δ 201.5, 165.4 (d, *J* = 251.6 Hz), 155.2, 137.1, 132.8, 131.6 (d, *J* = 9.3 Hz), 126.6, 121.6, 119.7, 116.2 (d, *J* = 21.7 Hz), 112.1, 66.5, 65.7, 50.3, 46.6, 43.6, 32.9, 29.6, 29.4, 27.8. HRMS (ESI) Calcd for $C_{22}H_{25}FNO_3$ (M+H)[+] 370.1818, found: 370.1833.

3.1.5 (1-(8-(2-Fluoroethoxy)-3-hydroxy-1,2,3,4-tetrahydronaphthalen-2-yl)piperidin-4-yl)(4-fluorophenyl)methanone (18a)

—Compound **17a** (74 mg, 0.2 mmol), 2-fluoroethyl tosylate (52 mg, 0.24 mmol) and Cs_2CO_3 (98 mg, 0.3 mmol) were mixed in THF (5 mL) and refluxed overnight. The reaction mixture was partitioned between ethyl acetate and water. After drying over anhydrous Na_2SO_4, the organic phase was concentrated and purified on silica gel column by CH_2Cl_2/ethyl acetate (1/1, v/v) to get a white solid **18a** (65 mg, 78%). Mp 149 – 152 °C. ^{1}H NMR (400 MHz, $CDCl_3$) δ 1.79 -1.95 (m, 4H), 2.47-2.61 (m, 2H), 2.72-2.99 (m, 5H), 3.10 (d, $J = 16.5$Hz, 1H), 3.24-3.35 (m, 2H), 3.84 (m, 1H), 4.18 (s, 1H), 4.27 (s, 1H), 4.72 (s, 1H), 4.88 (s, 1H), 6.65 (d, $J = 8.4$Hz, 1H), 6.76 (d, $J = 8.4$Hz, 1H), 7.08-7.19 (m, 3H), 8.00 (t, $J = 8.7$Hz, 2H). ^{13}C NMR (75.5 MHz, CD_3COCD_3) δ 200.5, 165.4 (d, $J = 254.2$ Hz), 156.3, 135.7, 132.8, 131.2 (d, $J = 9.2$ Hz), 126.6, 124.0, 121.5, 115.5 (d, $J = 22.0$ Hz), 108.3, 82.1 (d, $J = 168.4$ Hz), 67.4 (d, $J = 19.6$ Hz), 66.5, 65.2, 51.6, 44.6, 43.5, 38.2, 20.1; HRMS (ESI) Calcd for $C_{24}H_{28}F_2NO_3$ (M+H)[+] 416.2037, found: 416.2041. The free base was converted to oxalate salt as described above.

3.1.6 (1-(5-(2-Fluoroethoxy)-3-hydroxy-1,2,3,4-tetrahydronaphthalen-2-yl)piperidin-4-yl)(4-fluorophenyl)methanone (18b)

—Compound **18b** was obtained by using **17b** as the starting material, following the procedure for making **18a**. Mp 137 – 138 °C. ^{1}H NMR (400 MHz, $CDCl_3$) δ 1.79 -1.92 (m, 4H), 2.36-2.54 (m, 2H), 2.75-3.02 (m, 6H), 3.27 (s, 1H), 3.50(d, $J = 16.8$Hz, 2H), 3.84 (m, 1H), 4.11 (s, 1H), 4.24 (s, 1H), 4.67 (s, 1H), 4.83 (s, 1H), 6.66 (d, $J = 8.1$Hz, 1H), 6.74 (d, $J = 7.5$Hz, 1H), 7.07-7.17(m, 3H), 7.98 (t, $J = 8.7$Hz, 2H). ^{13}C NMR (75.5 MHz, CD_3COCD_3) δ 200.4, 165.4 (d, $J = 256.4$ Hz), 156.3, 136.8, 132.8 (d, $J = 3.0$ Hz), 131.1 (d, $J = 9.2$ Hz), 130.4, 123.2, 121.5, 115.6 (d, $J = 22.0$ Hz), 108.4, 82.1 (d, $J = 168.4$ Hz), 67.4 (d, $J = 19.8$ Hz), 66.1, 65.7, 51.4, 44.9, 43.6, 32.3, 26.3. HRMS (ESI) Calcd for $C_{24}H_{28}F_2NO_3$ (M+H)[+] 416.2032, found: 416.2029.

3.1.7 3-(4-(4-Fluorobenzoyl)piperidin-1-yl)-5-(2-fluoroethoxy)-1,2,3,4-tetrahydronaphthalen-2-yl acetate (19a)

—Racemic compound (±)-**18a** (140 mg, 0.337 mmol), acetic anhydride (200 μL) and pyridine (200 μL) were dissolved in CH_2Cl_2 (10 mL) and stirred at ambient temperature overnight. The product was extracted using ethyl acetate, and then dried over anhydrous Na_2SO_4. After solvent was removed under vacuum, the residue was purified on silica gel column by ethyl acetate/hexane (1/5 to 1/3, v/v) to afford (±)-**19a** as a white solid (148 mg, 96%). Mp 70 - 73 °C. ^{1}H NMR (400 MHz, $CDCl_3$) δ 1.58-1.86 (m, 4H), 2.10 (s, 3H), 2.45-2.76 (m, 3H), 2.80-3.20 (m, 7H), 4.02-4.25 (m, 3H), 4.65 (s, 1H), 4.80 (s, 1H), 6.57-6.74 (m, 2H), 7.01-7.15 (m, 3H), 7.95 (br s, 2H). ^{13}C NMR (75.5 MHz, CD_3OD) δ 202.0, 171.0, 156.2, 131.0, 130.9, 126.6, 121.1, 120.8, 115.4 (d, $J = 21.9$ Hz), 115.2, 108.6, 108.4, 81.9 (d, $J = 169.3$ Hz), 70.0, 66.2 (d, $J = 25.3$ Hz), 63.3, 49.5, 43.5, 37.9, 34.7, 29.0, 22.2, 21.1, 20.0. HRMS (ESI) Calcd for $C_{26}H_{30}F_2NO_4$ (M+H)[+] 458.2143, found: 458.2152.

3.1.8 (-)-(1-(8-(2-Fluoroethoxy)-3-hydroxy-1,2,3,4-tetrahydronaphthalen-2-yl)piperidin-4-yl)(4-fluorophen-yl)-methanone ((-)-18a)

—Enantiomers of (±)-**19a** (132 mg, 0.29 mmol) were separated by HPLC using a Chiralcel OD column (250 mm × 10 mm), 2-propanol/hexane (3/97, v/v) as mobile phase, flow rate of 4.0 mL/min, and UV wavelength at 254 nm) to give (-)-**19a** (53 mg, 40%) and (+)-**19a** (61 mg, 46%) respectively.

Each enantiopure compound was mixed with saturated Na_2CO_3 aqueous solution (3 mL) in EtOH (3 mL) separately and stirred for 72h at room temperature. Water (20 mL) was used to dilute the reaction mixture followed by extraction using CH_2Cl_2 (20 mL × 3). The combined organic phase was dried over anhydrous Na_2SO_4, and the solvent was removed under reduced pressure. The crude product was purified on silica gel column using ethyl acetate/hexane (1/1, v/v) to afford (-)-**18a** as a white solid (40 mg, 88% yield). ^{1}H NMR (400 MHz, CDCl$_3$) δ 8.00 (t, J = 8.0 Hz, 2H), 7.17 – 7.09 (m, 3H), 6.76 (d, J = 8.0 Hz, 1H), 6.65 (d, J = 8.0 Hz, 1H), 4.87 - 4.85 (m, 1H), 4.75 - 4.73 (m, 1H), 4.27 – 4.15 (m, 3H), 3.85 – 3.75 (m, 1H), 3.30 – 3.20 (m, 2H), 3.13 – 3.02 (m, 1H), 2.99 – 2.70 (m, 5H), 2.60 – 2.43 (m, 2H), 1.98 – 1.73 (m, 4H). ^{13}C NMR (100 MHz, CDCl$_3$) δ 200.9, 165.6 (d, J = 253.5 Hz), 156.1, 135.6, 132.3, 130.8, 126.7, 124.0, 122.0, 115.8 (d, J = 21.7 Hz), 108.1, 82.0 (d, J = 169.8 Hz), 67.2 (d, J = 20.2 Hz), 66.4, 65.1, 52.1, 44.3, 43.8, 37.9, 29.6, 29.2, 20.0. The free base of **(-)-18a** was converted to oxalate salt, Mp: 185.0-185.3 °C. The optical rotation of the oxalate salt was $[\alpha]_D^{20}$ = -37.1° (0.7 mg/mL in 1/1 acetonitrile/H$_2$O). HRMS (ESI) Calcd for $C_{24}H_{28}F_2NO_3$ (M+H)$^+$ 416.2032, found: 416.2022.

3.1.9 (+)-(1-(8-(2-Fluoroethoxy)-3-hydroxy-1,2,3,4-tetrahydronaphthalen-2-yl)pipe-ridin-4-yl)(4-fluorophenyl)-methanone ((+)-18a)—Starting with (+)-**19a** (58 mg), the procedure of making (-)-**18a** afforded compound (+)-**18a** as a yellow oil (44.0 mg, 83% yield). ^{1}H NMR (400 MHz, CDCl$_3$) δ 8.00 (t, J = 8.0 Hz, 2H), 7.17 – 7.09 (m, 3H), 6.76 (d, J = 8.0 Hz, 1H), 6.65 (d, J = 8.0 Hz, 1H), 4.87 - 4.85 (m, 1H), 4.75 - 4.73 (m, 1H), 4.27 – 4.15 (m, 3H), 3.85 – 3.75 (m, 1H), 3.30 – 3.20 (m, 2H), 3.13 – 3.02 (m, 1H), 2.99 – 2.70 (m, 5H), 2.60 – 2.43 (m, 2H), 1.98 – 1.73 (m, 4H). ^{13}C NMR (100 MHz, CDCl$_3$) δ 200.9, 165.6 (d, J = 253.4 Hz), 156.1, 135.6, 130.8, 126.7, 124.0, 122.0, 115.8 (d, J = 21.7 Hz), 108.2, 82.0 (d, J = 169.9 Hz), 67.2 (d, J = 20.2 Hz), 66.5, 65.1, 52.1, 44.3, 43.8, 37.9, 29.6, 29.2, 20.0. The free base was converted to oxalic salt, Mp: 191.0 – 192.2 °C. The optical rotation of (+)-**18a** was $[\alpha]_D^{20}$ = 38.4° (0.65 mg/mL in 1/1 acetonitrile/H$_2$O). HRMS (ESI) Calcd for $C_{24}H_{28}F_2NO_3$ (M+H)$^+$ 416.2032, found: 416.2021.

3.2 *In vitro* biological evaluation

3.2.1 VAChT binding affinity studies—Binding affinities of the new compounds were determined by competing them against 5 nM [^{3}H]vesamicol for binding to human VAChT present in synaptic-like microvesicles in postnuclear supernatant prepared from PC12$^{A123.7}$ cells.[50] Nonspecific binding was determined from samples that contained 1 μM of nonradioactive (±)-vesamicol. The test compounds were assayed in increments of 10-fold from 0.1 to 10,000 nM concentration. The surfaces of containers were pre-coated with Sigmacote (Sigma-Aldrich, MO). Samples containing 200 µg postnuclear supernatant in 200 μL of 110 mM potassium tartrate, 20 mM HEPES (pH 7.4 with KOH), 1 mM dithiothreitol and 0.02 % sodium azide were incubated at 22 °C for 24 h. A volume of 90 µL was filtered in duplicate through GF/F glass fiber filters coated with polyethylenimine and washed. Filter-bound radioactivity was determined by liquid scintillation spectrometry for 10 min per sample. Averaged data were fitted by regression with a rectangular hyperbola to estimate K_i. All compounds were independently assayed at least two times.

3.2.2 Sigma receptors binding affinity studies—The σ receptor binding affinity studies were performed following our previously reported procedure. [51, 52] The σ_1 receptor binding assays were performed in 96-well plates by incubating test compounds with approximately 300 μg protein of guinea pig brain membrane homogenates and 5 nM (+)-[^{3}H]pentazocine (1.30 GBq/μmol, Perkin Elmer, Boston, MA). Non-specific binding was determined from samples containing 10 μM cold haloperidol. The σ_2 receptor binding assays were similarly performed by incubating test compound(s) with rat liver membrane homogenates (~300 μg protein) and ~5 nM [^{3}H]DTG (2.15 GBq/μmol, Perkin Elmer, Boston, MA) in the presence of 1 μM (+)-pentazocine to block σ_1 sites. Non-specific binding was determined from samples that contained 10 μM of cold haloperidol. Data from the competitive inhibition experiments were modeled using nonlinear regression analysis to determine the concentration that inhibits 50% of the specific binding of the radioligand (IC_{50} value). Competitive binding curves were best fit to a one-site fit and gave pseudo-Hill coefficients of 0.6 – 1.0. K_i values were calculated using the method of Cheng and Prusoff [36] and are presented as the mean ± SEM. For these calculations, we used a K_d value of 7.89 nM for (+)-[^{3}H]pentazocine in guinea pig brains and a K_d value of 30.73 nM for [^{3}H]ditolylguanidine in rat livers.

3.3 Radiochemistry

3.3.1 Radiosynthesis of 1-[^{18}F]fluoro-2-tosyloxyethane ([^{18}F]20)—A sample of ~5.50 GBq [^{18}F]/fluoride was added to a reaction vessel containing Kryptofix 2.2.2 (6.5 - 7.0 mg). To the mixture, acetonitrile (3×1.0 mL) was added to remove azeotropically water using nitrogen gas to bubble though the mixture at ~110 °C. After all the water was removed, 1, 2-ethylene ditosylate (5.0 – 5.5 mg) was dissolved into acetonitrile (200 μL) under vortex, and then the solution was transferred to the reaction vessel containing [^{18}F]fluoride/Kryptofix /K_2CO_3. The reaction vessel was capped and the reaction mixture was briefly mixed, then heated about 10 min in an oil bath that was preheated to 110 °C. After reaction, the vessel was lifted up from the oil bath, the reaction mixture was diluted using 3.0 mL of HPLC mobile phase composed of 50/50 ratio of acetonitrile/0.1 M aqueous ammonium formate (pH ~6.5), and passed through an alumina Neutral Sep-Pak Plus cartridge. The crude product was then loaded onto an Agilent SB-C18 semi-preparative HPLC column (250 mm × 10 mm) with a UV detector set at 254 nm. The HPLC system was equipped with a 5 mL injection loop. At the flow rate of 4.0 mL/min, the retention time of the product was 9.5-10 min. The retention time of the precursor was 23-24 min. The product eluted from the HPLC was diluted using ~50 mL sterile water and then passed through a C-18 Sep-Pak Plus cartridge to trap [^{18}F]**20** on the Sep-Pak. Using ether (2.5 mL) to elute the radioactivity afforded [^{18}F]**20** (2.60-3.0 MBq, 60-75% radiochemistry yield, decay corrected to end of synthesis, EOS). The synthesis of [^{18}F]**20** took about 40 min.

3.3.2 Radiosynthesis of (-)-[^{18}F]18a—The upper ether layer of the eluted solution of [^{18}F]**20** was transferred into a vial first, and the bottom aqueous phase was extracted with an additional 1 mL of ether. The combined ether solution was passed through a set of two Sep-Pak Plus dry cartridges into a reaction vessel. After the ether was evaporated with a nitrogen stream at 25 °C, the solution of precursor (-)-**17a** (1.0 - 1.4 mg) in DMSO (200 μL), and Cs_2CO_3 (1.0 - 1.5 mg) were added to the abovementioned reaction vessel containing

[¹⁸F]**20**. The vessel was capped, vortexed, and then heated at 100 °C for 15 min. Subsequently, the residual was diluted with 3 mL HPLC mobile phase (35:65 acetonitrile/0.1 M ammonium formate buffer (pH ~4.5)) and loaded onto a semi-preparative HPLC system for purification. The HPLC system contains a 5 mL injection loop, an Agilent SB-C18 column, a UV detector at 254 nm and a radioactivity detector. With 35:65 acetonitrile/0.1 M ammonium formate buffer (pH ~4.5) as eluent, at 4.0 mL/min flow rate, the retention time of the product was 24 - 26 min, whereas the retention time of **(-)-17a** was 9 - 10 min. The product collection was diluted using sterile water (~50 mL) and then passed through a C18 Sep-Pak Plus cartridge. The trapped product was eluted using ethanol (0.6 mL), followed by 0.9% saline (5.4 mL). After sterile filtration into a glass vial, the **(-)-[¹⁸F]18a** was ready for quality control (QC) analysis and animal studies. To check the quality of the **-(-)-[¹⁸F]18a**, an aliquot of sample was co-injected with nonradiolabeled standard **(-)-18a** sample solution onto an analytical HPLC system equipped with an Agilent Zorbax SB-C18 column (250 × 4.6 mm) and UV absorbance at 254 nm; the mobile phase consisted of acetonitrile/0.1 M ammonium formate buffer (52/48, v/v). Under these conditions, the retention time of (-)-[¹⁸F]**18a** was ~ 5.0 min at a flow rate of 1.5 mL/min. For this step, the radiochemical purity was > 98%, the radiochemical yield was 50 - 60% (n > 20, decay corrected to EOS) and the specific activity was > 74 GBq/μmol (decay corrected to EOS). The synthesis of (-)-[¹⁸F]**18a** starting with [¹⁸F]**20** took about 80 min. The entire two-step procedure of making (-)-[¹⁸F]**18a** starting with K[¹⁸F]F took ~2.0 h and the radiochemical yield was 30 – 40%.

3.4 Biodistribution studies in rats

All animal experiments were conducted in compliance with the Guidelines for the Care and Use of Research Animals under protocols approved by Washington University's Animal Studies Committee. For the biodistribution studies, the solution of (-)-[¹⁸F]**18a** (~2.2 MBq/120 μL) in 10% ethanol in saline was injected via the tail vein into adult male SD rats under 2-3% isoflurane/oxygen anesthesia. At 5, 30, 60, and 120 min p.i. (n = 4 for each time point), the rats were euthanized under anesthesia. The whole brain was quickly harvested and dissected into regions of cerebellum, brain stem, thalamus, striatum, cortex and hippocampus; the remainder of the brain was also collected to determine the total brain uptake. Samples of blood, heart, lung, muscle, fat, pancreas, spleen, kidney, liver, and bone were also collected, and all the samples were counted in an automated Beckman Gamma 8000 well counter with a standard dilution of the injectate. Tissues were weighed and the %ID/g was calculated. The striatum/organ ratios were calculated using the striatal uptake (%ID/g) divided by the %ID/g of the different brain regions.

For the *ex vivo* autoradiography study, an adult male SD rat was injected with (-)-[¹⁸F]**18a** (~63.0 MBq) via the tail vein under anesthesia and euthanized at 60 min p.i. The brain was quickly removed, snap-frozen, and horizontal sections (100 μm) were sliced using a chrome brain matrix (Zivic Instruments Inc., Pittsburg, PA). Frozen slides were directly exposed to film in an imaging cassette (Fuji Photo Film Co., Tokyo, Japan) for 12 hrs at −80 °C in the dark. The distribution of radioactivity was visualized by a Fuji Bio-Imaging Analyzer FLA-7000 (Fuji Photo Film Co., Tokyo, Japan). Photo-stimulated luminescence (PSL) from the striatum and cerebellum was quantified using Multi Gauge v3.0 software (Fuji Photo

Film Co., Tokyo, Japan). Data were background-corrected, and expressed as photo-stimulated luminescence signals per square millimeter (PSL/mm^2).

3.5 *In vivo* microPET imaging

Three PET studies were performed on adult male cynomolgus monkeys (6-8 Kg) with a microPET Focus 220 scanner (Concorde/CTI/Siemens Microsystems, Knoxville, TN). The animals were fasted for 12 h prior to each PET study. The animals were initially anesthetized using an intramuscular injection with ketamine (10 - 20 mg/kg) and glycopyrrolate (0.013 - 0.017 mg/kg) and then transported to the PET scanner suit. Upon arrival, the animal was intubated with an endotracheal tube and anesthesia was maintained at 0.75 - 2.0% isoflurane/oxygen throughout the procedure. After intubation, a percutaneous venous catheter was placed for radiotracer injection. Core temperature was kept constant at 37 °C with a heated water blanket. In each microPET scanning session, the head was positioned supine in the adjustable head holder with the brain in the center of the field of view. A 10-min transmission scan was performed to check positioning; once confirmed, a 45 min transmission scan was obtained for attenuation correction. Subsequently, a 2 hr dynamic emission scan was acquired after administration of 296 - 410 MBq of (-)-[^{18}F]**18a** via the venous catheter. In the blocking studies, (-)-vesamicol (0.25 mg/kg) was administrated to the animal 5 min prior to the (-)-[^{18}F]**18a** injection via the venous catheter.

3.6 MicroPET image processing and analysis

PET scans were collected from 0 – 120 min with the following time frames: 3×1 min, 4×2 min, 3×3 min and 20×5 min. PET image reconstructed resolution was < 2.0 mm full width half maximum for all 3 dimensions at the center of the field of view. Emission data were corrected using individual attenuation and model-based scatter correction and reconstructed using filtered back projection. The first baseline PET image for each animal acted as the target image with the MPRAGE and subsequent PETs co-registered using automated image registration program AIR. All MPRAGE-based volume of interest (VOI) analyses were accomplished by experienced investigators. For quantitative analyses, three-dimensional ROIs (cerebellum and striatum) were transformed to the baseline PET space and then overlaid on all reconstructed PET images to obtain time-activity curves. Activity measures were standardized to body weight and dose of radioactivity injected to yield standardized uptake value (SUV).

3.7 Metabolite studies on NHP plasma

Arterial blood samples (1.2 - 1.5 mL) were collected at 5, 15 30, 60, 90, and 120 min post-injection of the radiotracer in a heparinized syringe.[41, 53] Aliquots of whole blood (1 mL) were counted in a well counter, then centrifuged to separate red blood cells from plasma. Aliquots of plasma (400 μL) were solvent deproteinated using 0.92 mL ice-cold methanol and separated by centrifugation. The supernatant was mixed with water (1/1, v/v) and the mixture was injected to a HPLC system for radioactive metabolite determination. The HPLC system consisted of an Agilent SB C-18 analytic HPLC column (250 mm × 4.6 mm, 5 μA) and an UV detector with wavelength set at 254 nm. The mobile phase was acetonitrile/0.1 M ammonium formate buffer (pH, ~ 4.5, 52/48, v/v), and the flow rate was 1.5 mL/min. The

HPLC fractions were collected at 1 min intervals for 16 min; each fraction was counted by a well counter to determine the radioactivity of each collection. The results were corrected for background radiation and physical decay.

To confirm if the major radioactive metabolite is able to enter into the brain, metabolite analysis was performed for the rat plasma samples post injection of (-)-[^{18}F] **18a**. 15 – 106 MBq of (-)-[^{18}F] **18a** was injected into male SD rats which were euthanized 5, 15, 30 and 60 min p.i. The rat plasma samples were prepared as described above. The rat brain tissue homogenate samples were prepared by following our published procedure,[41, 48] briefly, the whole brain was harvested and the excess blood was blotted; the brain tissue was homogenized on ice; acetonitrile (1.2 mL) was then added to extract the radioactivity and homogenize further. A 1.0 mL aliquot of this brain homogenate was centrifuged to remove the debris; 0.2 mL of the clear supernatant was diluted with 0.2 mL of distilled water to form the HPLC injection sample. The rat plasma and rat brain tissue samples were used for HPLC analysis following the procedure described above.

4. Conclusions

In this study, we successfully synthesized nine new carbonyl-containing fluorinated VAChT ligands. *In vitro* binding studies suggested that (-)-**18a** is a potent and selective candidate PET ligand. *Ex vivo* autoradiography studies and biodistribution studies in rodents and microPET studies in nonhuman primates suggest that (-)-[^{18}F]**18a** specifically accumulates in the striatum, the VAChT enriched region of the brain. Striatal uptake of (-)-[^{18}F]**18a** measured in monkeys using PET reached maximum uptake (SUV = 5.1) at 15 min p.i. More importantly, the striatal activity levels gradually decreased over time. Washout of the radioactivity from the nonspecific binding reference region, cerebellum, was much faster than in the target striatal regions. A blocking study using vesamicol strongly suggested that (-)-[^{18}F]**18a** specifically binds to VAChT in the striatal regions. Over all, (-)-[^{18}F]**18a** is a promising PET radiotracer candidate for quantifying VAChT levels *in vivo*. Currently an exploratory Investigational New Drug (IND) application has been approved by the Food and Drug Administration. The translational clinical investigation of (-)-[^{18}F]**18a** in normal control subjects and patients is in progress.

Acknowledgements

Abbreviations

Ac$_2$O	acetic anhydride
AD	Alzheimer disease

|	
BVM	benzovesamicol
calcd	calculated
CH$_2$Cl$_2$	dichloromethane
CNS	central nervous system
DMF	*N,N*-dimethylformamide
DMSO	dimethyl sulfoxide
[^{3}H]DTG	[^{3}H]ditolylguanidine
EOB	end of bombardment
EtOH	ethanol
[^{18}F]FEOBV	[^{18}F]fluoroethoxybenzovesamicol
HPLC	high performance liquid chromatography
HRMS	high resolution mass spectrometry
[^{123}I]IBVM	(-)-5-[^{123}I]iodobenzovesamicol
IC$_{50}$	half maximum inhibitory constant
MABV	5-(*N*-methyl-amino)benzo-vesamicol
NEFA	*N*-ethyl-fluoroacetamidobenzo-vesamicol
NHPs	nonhuman primates
PD	Parkinson Disease
PET	positron emission tomography
p.i.	post-injection
PSL	photo-stimulated luminescence
QC	quality control
SD	Sprague-Dawley
SPECT	single-photon emission computerized tomography
SUV	standardized uptake value
THF	tetrahydrofuran
TLC	thin layer chromatography
VAChT	Vesicular Acetylcholine Transporter

References and notes

1. Bohnen NI, Albin RL. The cholinergic system and Parkinson disease. Behav Brain Res. 2011; 221:564–573. [PubMed: 20060022]

2. Ransome MI, Hannan AJ. Behavioural state differentially engages septohippocampal cholinergic and GABAergic neurons in R6/1 Huntington's disease mice. Neurobiol Learn Mem. 2012; 97:261–270. [PubMed: 22261461]

3. Bohnen NI, Kaufer DI, Hendrickson R, Ivanco LS, Lopresti B, Davis JG, Constantine G, Mathis CA, Moore RY, DeKosky ST. Cognitive correlates of alterations in acetylcholinesterase in Alzheimer's disease. Neurosci Lett. 2005; 380:127–132. [PubMed: 15854764]

4. Schliebs R, Arendt T. The cholinergic system in aging and neuronal degeneration. Behav Brain Res. 2011; 221:555–563. [PubMed: 21145918]

5. Muller ML, Bohnen NI. Cholinergic dysfunction in Parkinson's disease. Curr Neurol Neurosci Rep. 2013; 13:377.

6. Smith R, Chung H, Rundquist S, Maat-Schieman ML, Colgan L, Englund E, Liu YJ, Roos RA, Faull RL, Brundin P, Li JY. Cholinergic neuronal defect without cell loss in Huntington's disease. Hum Mol Genet. 2006; 15:3119–3131. [PubMed: 16987871]

7. Jung YW, Van Dort ME, Gildersleeve DL, Wieland DM. A radiotracer for mapping cholinergic neurons of the brain. J Med Chem. 1990; 33:2065–2068. [PubMed: 2374138]

8. Kuhl DE, Minoshima S, Fessler JA, Frey KA, Foster NL, Ficaro EP, Wieland DM, Koeppe RA. *In vivo* mapping of cholinergic terminals in normal aging, Alzheimer's disease, and Parkinson's disease. Ann Neurol. 1996; 40:399–410. [PubMed: 8797529]

9. Efange SM. *In vivo* imaging of the vesicular acetylcholine transporter and the vesicular monoamine transporter. FASEB J. 2000; 14:2401–2413. [PubMed: 11099458]

10. Usdin TB, Eiden LE, Bonner TI, Erickson JD. Molecular biology of the vesicular ACh transporter. Trends Neurosci. 1995; 18:218–224. [PubMed: 7610492]

11. Brittain RT, Levy GP, Tyers MB. The neuromuscular blocking action of 2-(4-phenylpiperidino) cyclohexanol (AH 5183). Eur J Pharmacol. 1969; 8:93–99. [PubMed: 4243404]

12. Brittain RT, Levy GP, Tyers MB. Observations on the neuromuscular blocking action of 2-(4-phenylpiperidino)-cyclohexanol (AH 5183). Br J Pharmacol. 1969; 36:173p–174p.

13. Bahr BA, Parsons SM. Acetylcholine transport and drug inhibition kinetics in *Torpedo* synaptic vesicles. J Neurochem. 1986; 46:1214–1218. [PubMed: 3950625]

14. Bahr BA, Parsons SM. Demonstration of a receptor in *Torpedo* synaptic vesicles for the acetylcholine storage blocker L-*trans*-2-(4-phenyl[3,4-^{3}H]-piperidino)cyclohexanol. Proc Natl Acad Sci U S A. 1986; 83:2267–2270. [PubMed: 3457385]

15. Kaufman R, Rogers GA, Fehlmann C, Parsons SM. Fractional vesamicol receptor occupancy and acetylcholine active transport inhibition in synaptic vesicles. Mol Pharmacol. 1989; 36:452–458. [PubMed: 2550778]

16. Efange SM, Mach RH, Smith CR, Khare AB, Foulon C, Akella SK, Childers SR, Parsons SM. Vesamicol analogues as sigma ligands: Molecular determinants of selectivity at the vesamicol receptor. Biochem Pharmacol. 1995; 49:791–797. [PubMed: 7702637]

17. Shiba K, Ogawa K, Ishiwata K, Yajima K, Mori H. Synthesis and binding affinities of methylvesamicol analogs for the acetylcholine transporter and sigma receptor. Bioorg Med Chem. 2006; 14:2620–2626. [PubMed: 16434200]

18. Custers FG, Leysen JE, Stoof JC, Herscheid JD. Vesamicol and some of its derivatives: Questionable ligands for selectively labelling acetylcholine transporters in rat brain. Eur J Pharmacol. 1997; 338:177–183. [PubMed: 9456000]

19. Haigh JR, Noremberg K, Parsons SM. Acetylcholine active transport by rat brain synaptic vesicles. Neuroreport. 1994; 5:773–776. [PubMed: 8018848]

20. Giboureau N, Som IM, Boucher-Arnold A, Guilloteau D, Kassiou M. PET radioligands for the vesicular acetylcholine transporter (VAChT). Curr Top Med Chem. 2010; 10:1569–1583. [PubMed: 20583990]

21. Rogers GA, Parsons SM, Anderson DC, Nilsson LM, Bahr BA, Kornreich WD, Kaufman R, Jacobs RS, Kirtman B. Synthesis, in vitro acetylcholine-storage-blocking activities, and biological properties of derivatives and analogues of trans-2-(4-phenylpiperidino)cyclohexanol (vesamicol). J Med Chem. 1989; 32:1217–1230. [PubMed: 2724295]

22. Rogers GA, Parsons SM. Photoaffinity labeling of the vesamicol receptor of cholinergic synaptic vesicles. Biochemistry. 1993; 32:8596–8601. [PubMed: 8357803]

23. Rogers GA, Kornreich WD, Hand K, Parsons SM. Kinetic and equilibrium characterization of vesamicol receptor-ligand complexes with picomolar dissociation constants. Mol Pharmacol. 1993; 44:633–641. [PubMed: 8371715]

24. Kuhl DE, Koeppe RA, Fessler JA, Minoshima S, Ackermann RJ, Carey JE, Gildersleeve DL, Frey KA, Wieland DM. *In vivo* mapping of cholinergic neurons in the human brain using SPECT and IBVM. Journal of Nuclear Medicine. 1994; 35:405–410.

25. Jung YW, Frey KA, Mulholland GK, del Rosario R, Sherman PS, Raffel DM, Van Dort ME, Kuhl DE, Gildersleeve DL, Wieland DM. Vesamicol receptor mapping of brain cholinergic neurons with radioiodine-labeled positional isomers of benzovesamicol. J Med Chem. 1996; 39:3331–3342. [PubMed: 8765517]

26. Lamare F, Mazere J, Attila M, Mayo W, De Clermont-Gallerande H, Meissner W, Fernandez P, Allard M. Improvement of *in vivo* quantification of [^{123}I]-iodobenzovesamicol in single-photon emission computed tomography/computed tomography using anatomic image to brain atlas nonrigid registration. Mol Imaging. 2013; 12:288–299. [PubMed: 23759370]

27. Mazere J, Meissner WG, Sibon I, Lamare F, Tison F, Allard M, Mayo W. [^{123}I]-IBVM SPECT imaging of cholinergic systems in multiple system atrophy: A specific alteration of the ponto-thalamic cholinergic pathways (Ch5-Ch6). Neuroimage Clin. 2013; 3:212–217. [PubMed: 24179865]

28. Meikle SR, Kench P, Kassiou M, Banati RB. Small animal SPECT and its place in the matrix of molecular imaging technologies. Phys Med Biol. 2005; 50:R45–61. [PubMed: 16264248]

29. Mulholland GK, Jung Y-W, Wieland DM, Kilbourn MR, Kuhl DE. Synthesis of [^{18}F]fluoroethoxy-benzovesamicol, a radiotracer for cholinergic neurons. J Labelled Comp Radiopharm. 1993; 33:583–591.

30. Mulholland GK, Wieland DM, Kilbourn MR, Frey KA, Sherman PS, Carey JE, Kuhl DE. [^{18}F]Fluoroethoxy-benzovesamicol, a PET radiotracer for the vesicular acetylcholine transporter and cholinergic synapses. Synapse. 1998; 30:263–274. [PubMed: 9776130]

31. Kilbourn MR, Hockley B, Lee L, Sherman P, Quesada C, Frey KA, Koeppe RA. Positron emission tomography imaging of (*2R,3R*)-5-[^{18}F]fluoroethoxybenzovesamicol in rat and monkey brain: A radioligand for the vesicular acetylcholine transporter. Nuc Med Biol. 2009; 36:489–493.

32. Petrou M, Frey KA, Kilbourn MR, Scott PJ, Raffel DM, Bohnen NI, Muller ML, Albin RL, Koeppe RA. *In vivo* imaging of human cholinergic nerve terminals with (–)-5-^{18}F-fluoroethoxybenzovesamicol: Biodistribution, dosimetry, and tracer kinetic analyses. J Nuc Med. 2014; 55:396–404.

33. Parent MJ, Bedard MA, Aliaga A, Minuzzi L, Mechawar N, Soucy JP, Schirrmacher E, Kostikov A, Gauthier SG, Rosa-Neto P. Cholinergic depletion in Alzheimer's disease shown by [^{18}F]FEOBV autoradiography. Int J Mol Imaging. 2013; 2013:205045. [PubMed: 24324884]

34. Parent MJ, Cyr M, Aliaga A, Kostikov A, Schirrmacher E, Soucy JP, Mechawar N, Rosa-Neto P, Bedard MA. Concordance between *in vivo* and postmortem measurements of cholinergic denervation in rats using PET with [^{18}F]FEOBV and choline acetyltransferase immunochemistry. EJNMMI Res. 2013; 3:70. [PubMed: 24103360]

35. Efange SM, Khare AB, von Hohenberg K, Mach RH, Parsons SM, Tu Z. Synthesis and in vitro biological evaluation of carbonyl group-containing inhibitors of vesicular acetylcholine transporter. J Med Chem. 2010; 53:2825–2835. [PubMed: 20218624]

36. Tu Z, Efange SM, Xu J, Li S, Jones LA, Parsons SM, Mach RH. Synthesis and in vitro and *in vivo* evaluation of ^{18}F-labeled positron emission tomography (PET) ligands for imaging the vesicular acetylcholine transporter. J Med Chem. 2009; 52:1358–1369. [PubMed: 19203271]

37. Tu Z, Wang W, Cui J, Zhang X, Lu X, Xu J, Parsons SM. Synthesis and evaluation of in vitro bioactivity for vesicular acetylcholine transporter inhibitors containing two carbonyl groups. Bioorg Med Chem. 2012; 20:4422–4429. [PubMed: 22739089]

38. Li J, Zhang X, Zhang Z, Padakanti PK, Jin H, Cui J, Li A, Zeng D, Rath NP, Flores H, Perlmutter JS, Parsons SM, Tu Z. Heteroaromatic and aniline derivatives of piperidines as potent ligands for vesicular acetylcholine transporter. J Med Chem. 2013; 56:6216–6233. [PubMed: 23802889]

39. Liu H, Jin H, Li J, Zhang X, Kaneshige K, Parsons SM, Perlmutter JS, Tu Z. In vitro and ex vivo characterization of (−)-TZ659 as a ligand for imaging the vesicular acetylcholine transporter. Eur J Pharmacol. 2015; 752:18–25. [PubMed: 25678250]

40. Padakanti PK, Zhang X, Li J, Parsons SM, Perlmutter JS, Tu Z. Syntheses and radiosyntheses of two C-11 labeled potent and selective radioligands for imaging vesicular acetylcholine transporter. Mol Imaging Biol. 2014:1–8. [PubMed: 24037176]

41. Padakanti PK, Zhang X, Jin H, Cui J, Wang R, Li J, Flores HP, Parsons SM, Perlmutter JS, Tu Z. In vitro and *in vivo* characterization of two C-11-labeled PET tracers for vesicular acetylcholine transporter. Mol Imaging Biol. 2014

42. Roberts MJ, Bentley MD, Harris JM. Chemistry for peptide and protein PEGylation. Adv Drug Deliv Rev. 2002; 54:459–476. [PubMed: 12052709]

43. Harris JM, Chess RB. Effect of pegylation on pharmaceuticals. Nat Rev Drug Discov. 2003; 2:214–221. [PubMed: 12612647]

44. Stephenson KA, Chandra R, Zhuang ZP, Hou C, Oya S, Kung MP, Kung HF. Fluoro-pegylated (FPEG) imaging agents targeting A aggregates. Bioconjug Chem. 2007; 18:238–246. [PubMed: 17226978]

45. Wang W, Cui J, Lu X, Padakanti PK, Xu J, Parsons SM, Luedtke RR, Rath NP, Tu Z. Synthesis and in vitro biological evaluation of carbonyl group-containing analogues for 1 receptors. J Med Chem. 2011; 54:5362–5372. [PubMed: 21732626]

46. Wenzel B, Sorger D, Heinitz K, Scheunemann M, Schliebs R, Steinbach J, Sabri O. Structural changes of benzylether derivatives of vesamicol and their influence on the binding selectivity to the vesicular acetylcholine transporter. Eur J Med Chem. 2005; 40:1197–1205. [PubMed: 16095762]

47. Scheunemann M, Sorger D, Wenzel B, Heinitz K, Schliebs R, Klingner M, Sabri O, Steinbach J. Synthesis of novel 4- and 5-substituted benzyl ether derivatives of vesamicol and in vitro evaluation of their binding properties to the vesicular acetylcholine transporter site. Bioorg Med Chem. 2004; 12:1459–1465. [PubMed: 15018919]

48. Paxinos, G.; Watson, C. The Rat Brain in Stereotaxic Coordinates. 4th ed.. Academic Press, Inc.; San Diego, CA: 1998.

49. Gilmor ML, Nash NR, Roghani A, Edwards RH, Yi H, Hersch SM, Levey AI. Expression of the putative vesicular acetylcholine transporter in rat brain and localization in cholinergic synaptic vesicles. J Neurosci. 1996; 16:2179–2190. [PubMed: 8601799]

50. Zea-Ponce Y, Mavel S, Assaad T, Kruse SE, Parsons SM, Emond P, Chalon S, Giboureau N, Kassiou M, Guilloteau D. Synthesis and in vitro evaluation of new benzovesamicol analogues as potential imaging probes for the vesicular acetylcholine transporter. Bioorg Med Chem. 2005; 13:745–753. [PubMed: 15653342]

51. Tu Z, Xu J, Jones LA, Li S, Dumstorff C, Vangveravong S, Chen DL, Wheeler KT, Welch MJ, Mach RH. Fluorine-18-labeled benzamide analogues for imaging the 2 receptor status of solid tumors with positron emission tomography. J Med Chem. 2007; 50:3194–3204. [PubMed: 17579383]

52. Xu J, Tu Z, Jones LA, Vangveravong S, Wheeler KT, Mach RH. [^{3}H]*N*-[4-(3,4-dihydro-6,7-dimethoxyisoquinolin-2(1*H*)-yl)butyl]-2-methoxy-5-methylbenzamide: A novel sigma-2 receptor probe. Eur J Pharmacol. 2005; 525:8–17. [PubMed: 16289030]

53. Tu Z, Fan J, Li S, Jones LA, Cui J, Padakanti PK, Xu J, Zeng D, Shoghi KI, Perlmutter JS, Mach RH. Radiosynthesis and *in vivo* evaluation of [^{11}C]MP-10 as a PET probe for imaging PDE10A in rodent and non-human primate brain. Bioorg Med Chem. 2011; 19:1666–1673. [PubMed: 21315609]
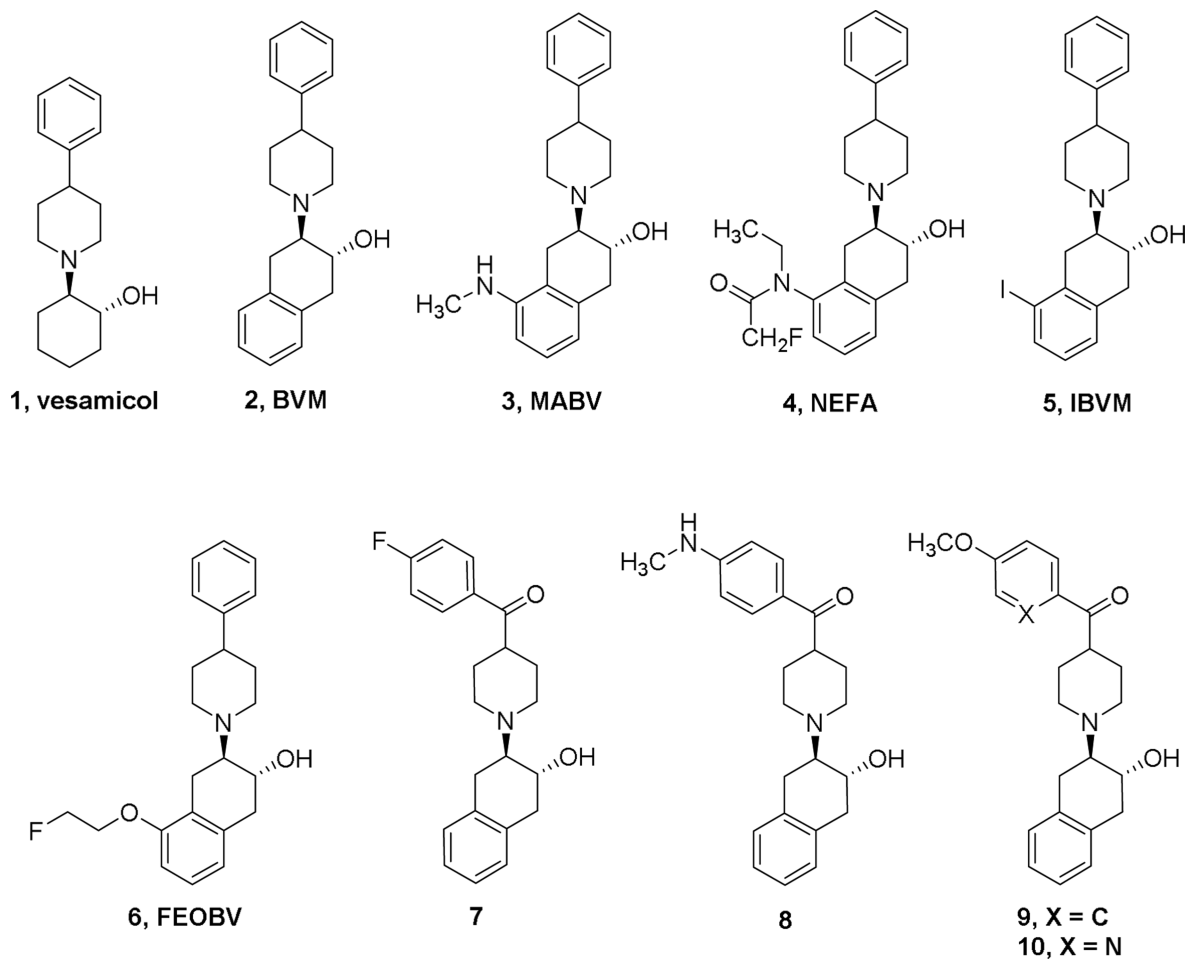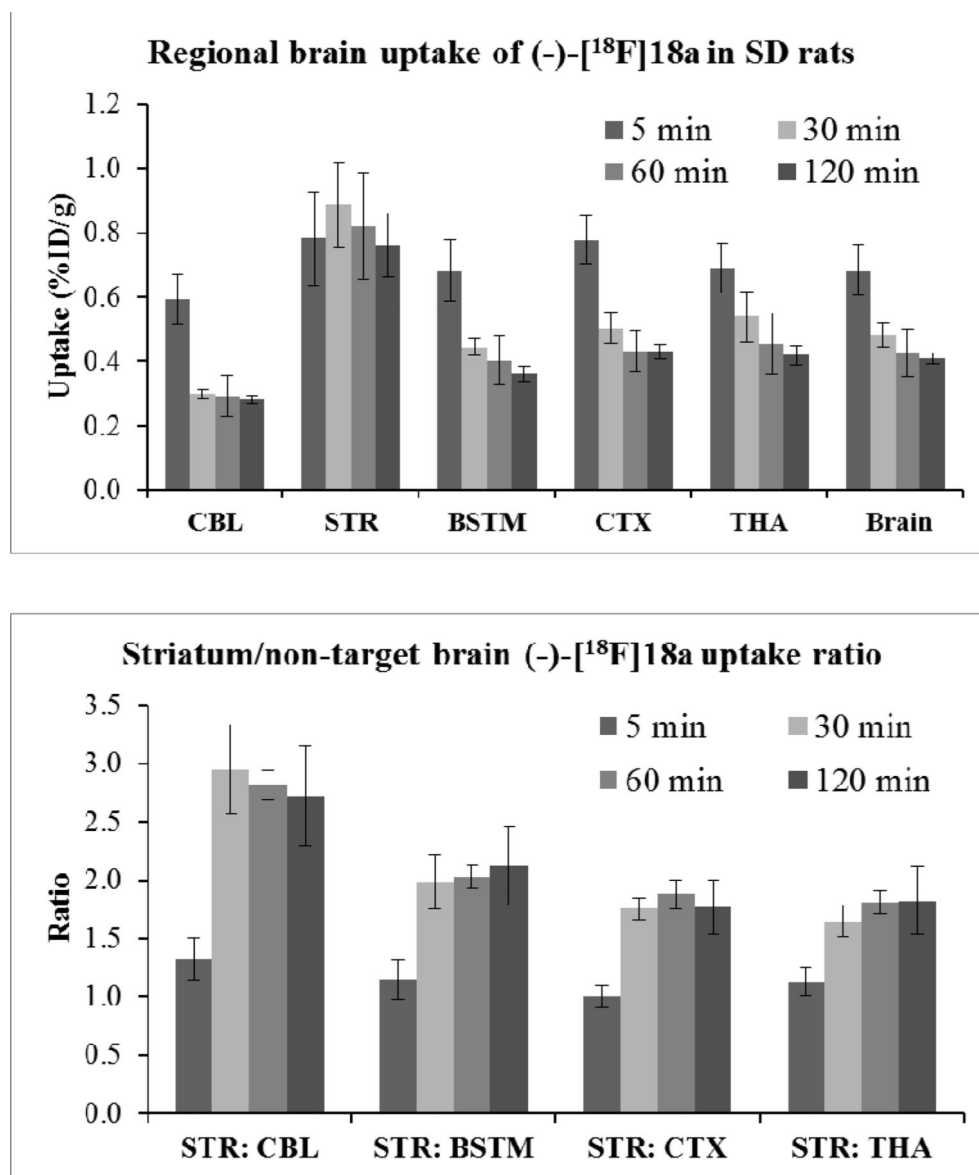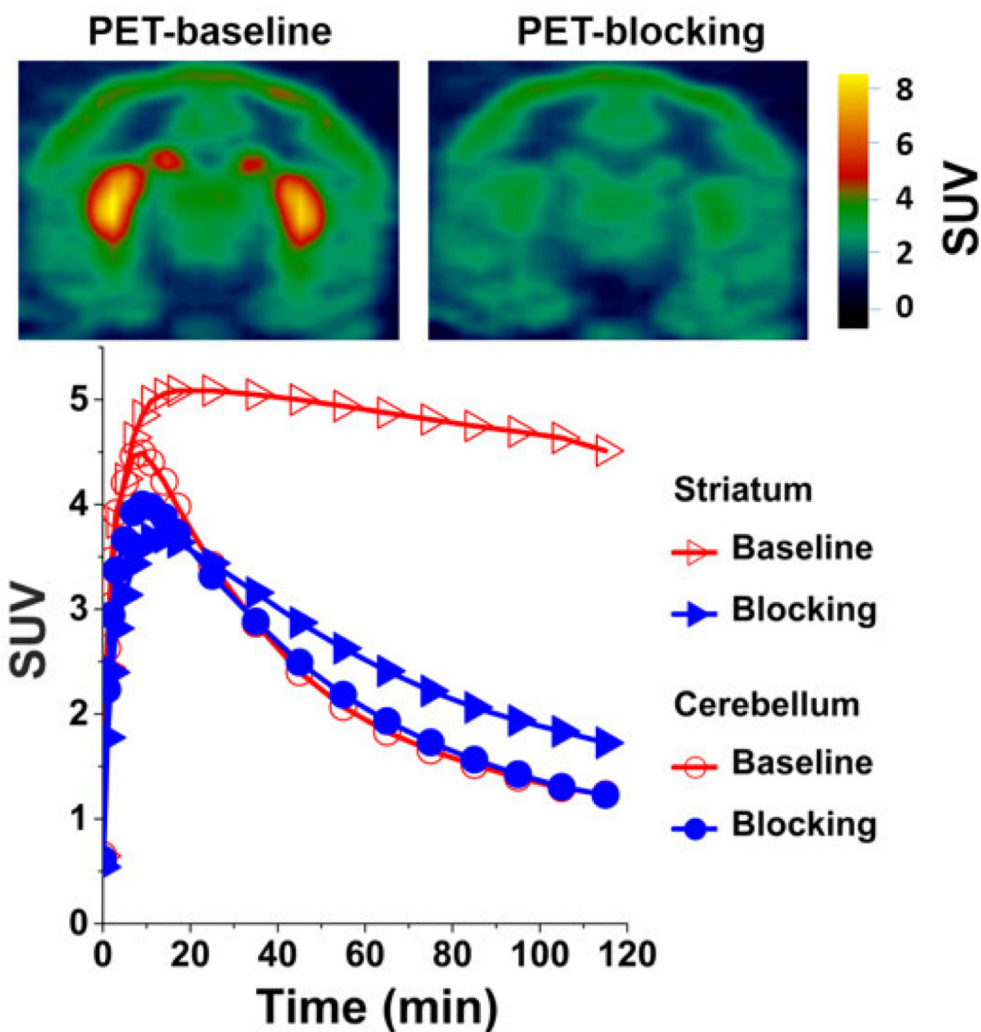
Figure 1.
Vesamicol, BVM and their derivatives.
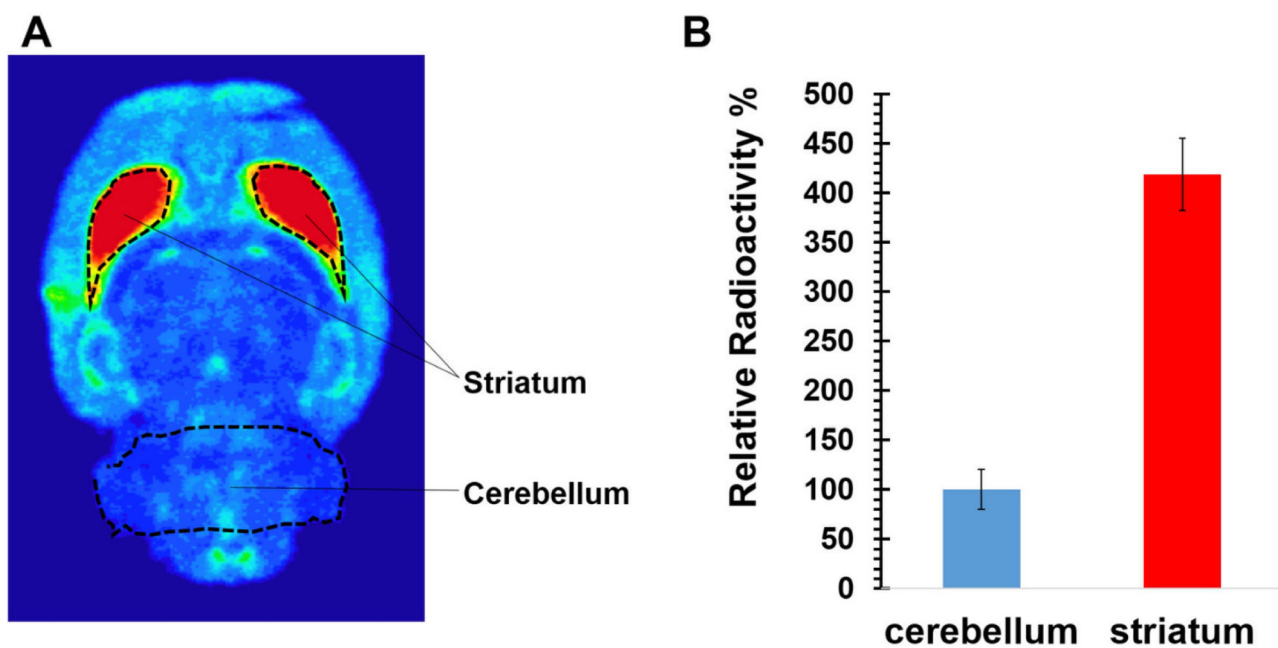
Figure 2.
Autoradiography of (-)-[^{18}F]**18a** in the male Sprague-Dawley (SD) rat brain. A). The representative horizontal slice (100 μm thick) of the SD rat brain shows the highest accumulation of radioactivity in the VAChT enriched striatal regions. B). Quantification of autoradiography from entire 30 brain slices indicates a striatum-to-cerebellum ratio of 4.19 ± 0.37 at 60 min post-injection. Histograms are the average of relative radioactivity of 30 brain slices. Error bars are the standard derivations.

Figure 3.
Regional brain uptake and striatum/organ ratio of (-)-[18F]**18a** in male SD rats. Both figures showed the radioactivity retention was the highest in the striatum at 30, 60 and 120 min p.i., while the radioactivity was quickly washed out in other brain regions. CBL: cerebellum; STR, striatum; BSTM, brain stem; CTX, cortex; THA, thalamus.

Figure 4.
Representative microPET images of (-)-[^{18}F]**18a** in cynomolgus monkey brain. **Upper panel:** PET image (left) at baseline condition and PET image, pretreated the animals using 0.25 mg/kg (-)-vesamicol 5 min prior to injection of the radiotracer (right). High uptake of (-)-[^{18}F]**18a** in striatum produced clear visualization of striatum (putamen and caudate) in the baseline condition. The pretreatment using 0.25 mg/kg (-)-vesamicol significantly reduced the uptake of (-)-[^{18}F]**18a** in the striatum (right). **Lower panel:** time tissue-activity curves for cerebellum (red open circles), striatum (red open triangles) at baseline condition, cerebellum (blue filled circles), and striatum (blue filled triangles) at the condition that animal was pretreated using 0.25 mg/kg (-)-vesamicol. SUV: standardized uptake value.
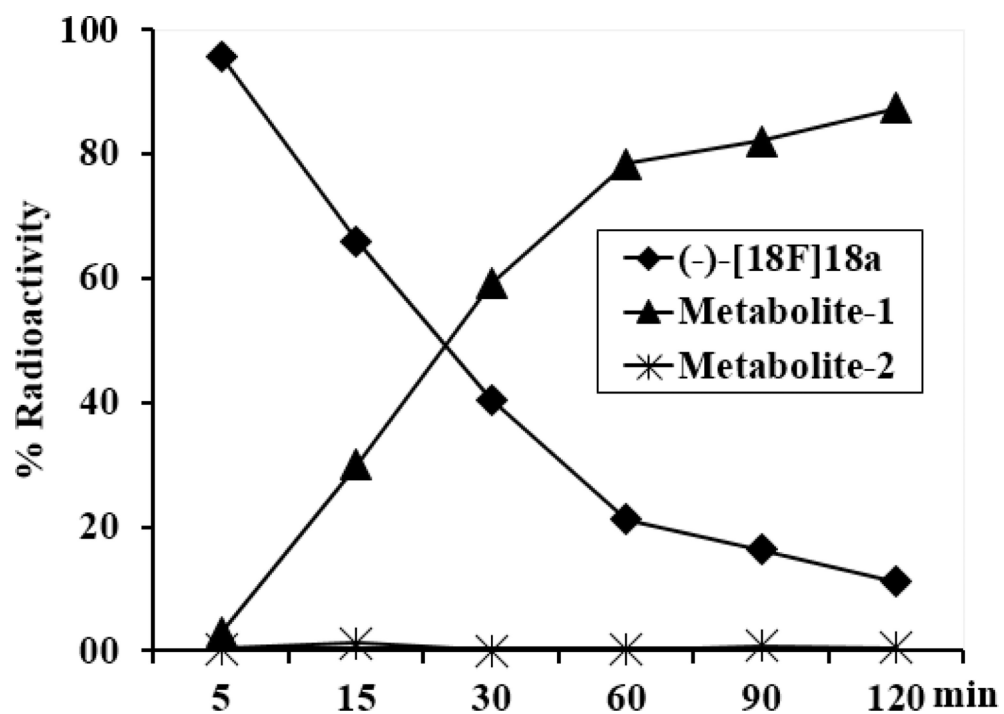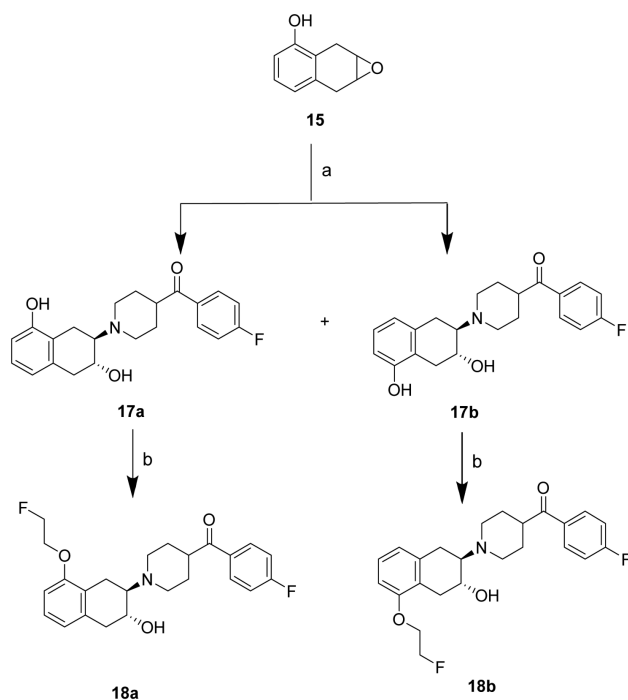
Figure 5.
Radiometabolite analysis of NHP arterial plasma samples post injection of (-)-[^{18}F]**18a**. The black diamonds represent the percentage intact radioactive parent compound at 5, 15, 30, 60, 90, and 120 min p.i.
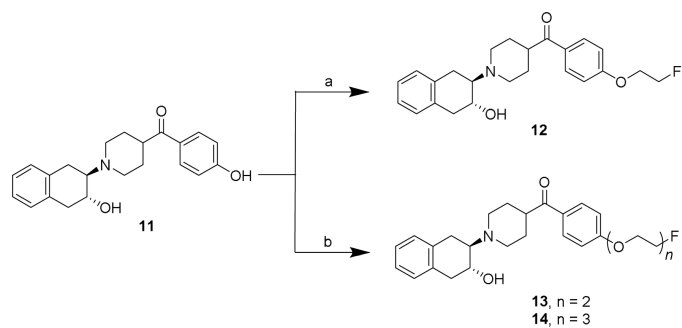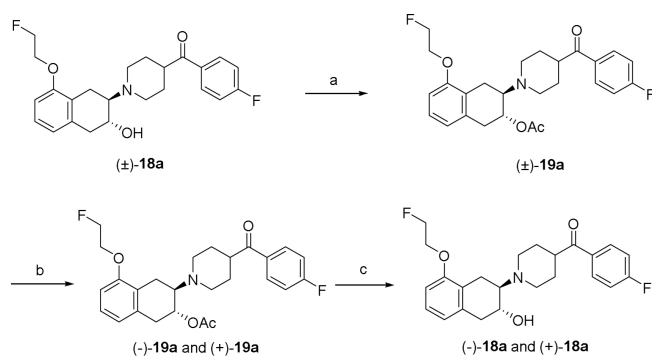
Reagents and conditions: a) $BrCH_2CH_2F$, K_2CO_3, acetone, reflux, 12 h, 77%; b) $Ts(OCH_2CH_2)_nF$, K_2CO_3, DMF, rt, 12 h, 78% for (±)-**13** and 41% for (±)-**14**.
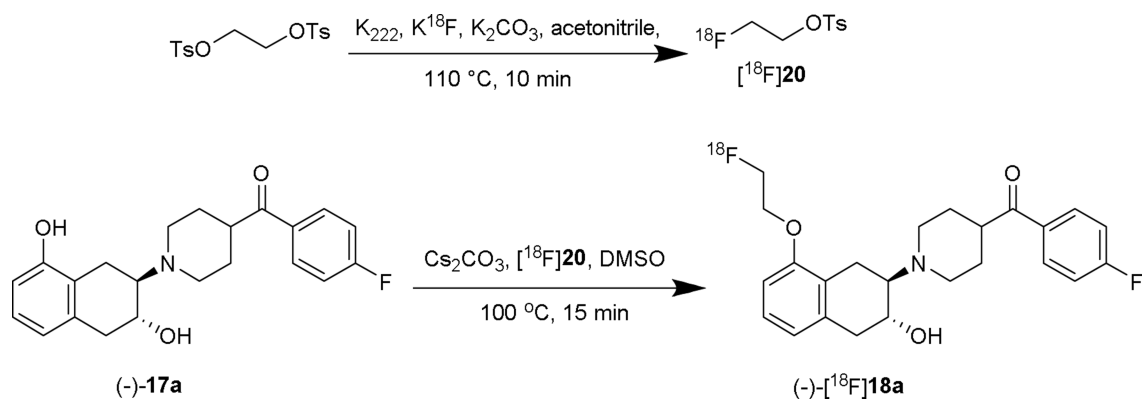
Scheme 1.
Syntheses of compounds **12 - 14**

Reagents and conditions: a) (4-fluorophenyl)(piperidin-4-yl)methanone (**16**), Et$_3$N, EtOH, 60 °C, 2d; b) TsOCH$_2$CH$_2$F, Cs$_2$CO$_3$, THF, reflux, overnight.

Scheme 2.
Syntheses of compounds **18a** and **18b**

Reagents and conditions: a) Ac₂O, pyridine, CH₂Cl₂, rt, overnight; b) separation of enantiomers of (±)-**19a** on chiral HPLC: Chiralcel OD semi-preparative column, mobile phase: 3% 2-propanol in hexanes; flow rate: 4.0 mL/min; c) sat. Na₂CO₃: EtOH 1:1, rt, 3 d.

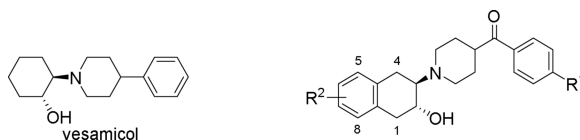**Scheme 3.**
Chiral separation of (±)-**18a**

Scheme 4.
Radiosynthesis of (-)-[^{18}F]**18a**

Table 1

Binding affinities of the fluoro-containing VAChT inhibitors

Ligands	R^1	R^2	$K_{i\text{-VAChT}}$	$K_{i\text{-}\sigma1}$	$K_{i\text{-}\sigma2}$	VAChT/ σ1	VAChT/ σ2	Log $P*^a$
Vesamicol*[b]			20.00	73.80	346.0	3.69	17.30	1.40
FBBV*[c]	H	H	2.70 ± 0.40	191.1 ± 57.7	251.3 ± 39.2	71	93	2.99
12	FCH_2CH_2O	H	1.74 ± 0.32	13.23 ± 0.20	1,885 ± 239	7.60	1083	3.15
13	$F(CH_2CH_2O)_2$	H	0.87 ± 0.09	1,580 ± 46	8,200 ± 97	1800	9300	2.79
14	$F(CH_2CH_2O)_3$	H	1.23 ± 0.09	>10,000	>10,000	>8,000	>9,000	2.43
17a	F	5-OH	4.64 ± 0.32	8,640 ± 974	1,851 ± 408	1,862	398.0	2.63
17b	F	8-OH	56.20 ± 4.08	28.70 ± 4.10	2,600 ± 178	0.51	46.30	2.59
18a	F	5-OCH_2CH_2F	1.55 ± 0.18	821 ± 34	>10,000	529	>6000	3.45
(+)-18a	F	5-OCH_2CH_2F	13.00 ± 2.19	>10,000	7,800 ± 882	1022	600.0	3.45
(−)-18a	F	5-OCH_2CH_2F	0.59 ± 0.06	>10,000	>10,000	>100,00	>10,000	3.45
18b	F	8-OCH_2CH_2F	92.80 ± 22.20	>10,000	7,145 ± 549	667.0	77.00	3.47

[a] Calculated value at pH = 7.4 by ACD/I-Lab ver. 7.0 (Advanced Chemistry Development, Inc., Canada).

[b] Reference 37.

[c] Reference 36.

Table 2

Biodistribution of (–)-[^{18}F]18a in male Sprague-Dawley rats[a]

Organs	5 min	30 min	60 min	120 min
Blood	0.209 ± 0.029	0.270 ± 0.033	0.338 ± 0.088	0.356 ± 0.019
Heart	0.706 ± 0.170	0.390 ± 0.031	0.357 ± 0.068	0.336 ± 0.016
Lung	2.255 ± 0.415	0.973 ± 0.107	0.738 ± 0.087	0.551 ± 0.070
Muscle	0.171 ± 0.055	0.258 ± 0.025	0.253 ± 0.044	0.235 ± 0.010
Fat	0.144 ± 0.054	0.324 ± 0.071	0.548 ± 0.354	0.560 ± 0.135
Pancreas	1.202 ± 0.323	1.200 ± 0.347	1.324 ± 0.346	0.819 ± 0.367
Spleen	1.265 ± 0.452	0.685 ± 0.082	0.505 ± 0.069	0.376 ± 0.034
Kidney	2.363 ± 0.520	0.883 ± 0.068	0.604 ± 0.092	0.489 ± 0.052
Liver	1.065 ± 0.121	0.523 ± 0.044	0.456 ± 0.122	0.382 ± 0.029
Bone	0.426 ± 0.086	0.369 ± 0.020	0.403 ± 0.095	0.537 ± 0.035
Total brain	0.684 ± 0.079	0.482 ± 0.037	0.425 ± 0.075	0.409 ± 0.016

[a]%ID/g values (mean ± SD) with 4 rats per group